Supporting Information for

Controllable Growth of Conducting Polymers Shell for Constructing High-Quality Organic/Inorganic Core/Shell Nanostructures and Their Optical-Electrochemical Applications

Xinhui Xia,[†‡] Dongliang Chao,[†] Xiaoying Qi,[§] Qinqin Xiong, [‡] Yongqi, Zhang, [‡] Jiangping Tu, [‡] Hua Zhang[§] and Hong Jin Fan[†,*]

[†] *Division of Physics and Applied Physics, School of Physical and Mathematical Sciences, Nanyang Technological University, Singapore 637371, Singapore,*

[§] *School of Materials Science & Engineering, Nanyang Technological University, Singapore 637371, Singapore,*

[‡] *State Key Laboratory of Silicon Materials, Key Laboratory of Advanced Materials and Applications for Batteries of Zhejiang Province, and Department of Materials Science and Engineering, Zhejiang University, Hangzhou 310027, China*

* Address correspondence to fanhj@ntu.edu.sg (H.J. F)

Methods and Materials

Preparation of Co_3O_4/PANI Core/Shell Nanowire Arrays. Firstly, self-supported Co_3O_4 nanowire arrays were prepared by a facile hydrothermal synthesis method.[1] The reaction solution was obtained by mixing 1.5 mmol of $Co(NO_3)_2$, 3 mmol NH_4F and 7.5 mmol of $CO(NH_2)_2$ in 50 mL of distilled water and then transferred into Teflon-lined stainless steel autoclave liners. Carbon cloth substrates (2×6 cm^2 in sizes) were immersed into the reaction solution. Top sides of the substrates were uniformly coated with a polytetrafluoroethylene tape to prevent the solution contamination. The liner was sealed in a stainless steel autoclave and maintained at 110 ºC for 5 h, and then cooled down to room temperature. The samples were collected and rinsed with distilled water several times. Finally, the samples were annealed at 350 ºC in normal purity argon for 2 h to obtain self-supported Co_3O_4 nanowire arrays. The reactions involved may be illustrated as follows.

$$Co^{2+} + xF^- \rightarrow [NiF_x]^{(x-2)-} \quad (1)$$

$$H_2NCoNH_2 + H_2O \rightarrow 2NH_3 + CO_2 \quad (2)$$

$$CO_2 + H_2O \rightarrow CO_3^{2-} + 2H^+ \quad (3)$$

$$NH_3 \cdot H_2O \rightarrow NH_4^+ + OH^- \quad (4)$$

$$2[CoF_x]^{(x-2)-} + CO_3^{2-} + 2OH^- + nH_2O \rightarrow Co_2(OH)_2CO_3 \cdot nH_2O + 2xF^- \quad (5)$$

During the annealing process:

$$3Co_2(OH)_2CO_3 \cdot nH_2O + O_2 \rightarrow 2Co_3O_4 + (3n+3)H_2O + 3CO_2 \quad (6)$$

The Co_3O_4 nanowire consists of numerous interconnected nanoparticles and presents a rough appearance with a large quantity of mesoporous structures, which is ascribed to the successive release and loss of CO_2 and H_2O during the thermal decomposition of $Co_2(OH)_2CO_3$ precursor.

Then the Co_3O_4 nanowire arrays were acted the backbone for the growth of PANI shell. Electrolyte for electro-polymerization of PANI was obtained by dissolving 0.5 ml aniline into 100 ml of 0.01 M H_2SO_4 solution. The electro-polymerization of PANI was carried out in a three-compartment system, the above Co_3O_4 nanowire arrays electrode as the working electrode, Ag/AgCl as the reference electrode and a Pt foil as the counter-electrode. The PANI film was deposited by applying constant anodic current density of 2.5 mA cm^{-2}. The

coaxial and branched Co_3O_4/PANI core/shell nanowire arrays were obtained when applying time for 500 s and 1500 s, respectively.

Preparation of TiO_2/PANI Core/Shell Nanorod Arrays. Firstly, self-supported TiO_2 nanorod arrays on transparent conductive fluorine-doped tin oxide (FTO) and carbon cloth were prepared by a facile hydrothermal synthesis method.[2] The reaction solution was prepared by adding 0.8 mL of titanium butoxide to a well-mixed solution containing 30 mL of HCl and 30 mL of H_2O, and then the whole mixture was stirred for another 10 min until the solution became clear. Afterward, the reaction solution was poured into a Teflon-liner stainless steel autoclave with the FTO substrates or carbon cloth placed at an angle against the wall. Hydrothermal growth was conducted at 150 °C for 2 h in an electric oven. Afterward, the FTO substrates were rinsed with deionized water and annealed 450 °C for 1 h in ambient air. Then, the self-supported TiO_2 nanorod arrays were used as the scaffold for PANI shell growth to obtain coaxial and branched TiO_2/PANI core/shell nanorod arrays as the same preparation parameters and methods mentioned above.

Preparation of Co_3O_4/PANI Core/Shell Nanoflake Arrays. Firstly, the porous Co_3O_4 nanoflake arrays were prepared by another facile hydrothermal synthesis method as follows.[3] The reaction solution was composed of 5 mmol of $Co(NO_3)_2$ and 10 mmol HMT (hexamethylene tetramine) in 50 mL of distilled water and then transferred into Teflon-lined stainless steel autoclave liners. Nickel foam substrates (2×6 cm^2 in sizes) were immersed into the reaction solution. After 8 h growth at 95 ^oC, the samples were annealed at 300 ^oC in normal purity argon for 2 h to obtain self-supported porous Co_3O_4 nanoflake arrays. Then, the coaxial and branched Co_3O_4/PANI core/shell nanoflake arrays were fabricated as the same preparation parameters and methods mentioned above.

Preparation of NiO/PANI Core/Shell Nanoflake Arrays. Firstly, the porous NiO nanoflake arrays were prepared by a facile hydrothermal synthesis method as follows.[4] The reaction solution was composed of 5 mmol of $Ni(NO_3)_2$ and 10 mmol HMT (hexamethylene tetramine) in 50 mL of distilled water and then transferred into Teflon-lined stainless steel autoclave liners. Nickel foam substrates (2×6 cm^2 in sizes) were immersed into the reaction solution. After 8 h growth at 95 ^oC, the samples were annealed at 300 ^oC in normal purity argon for 2 h to obtain self-supported porous NiO nanoflake arrays. Then, the coaxial and branched NiO/PANI core/shell nanoflake arrays were fabricated as the same preparation parameters and methods mentioned above.

Preparation of Co_3O_4/PEDOT Core/Shell Nanowire Arrays. The Co_3O_4 nanowire arrays were fabricated as above hydrothermal method. Then the Co_3O_4 nanowire arrays acted as the skeleton for the electrochemical growth of PEDOT as follows. The electro-polymerization of PEDOT was carried out by constant current deposition of 2.5 mA cm^{-2} in an acetonitrile solution of 10 mM 3,4-ethylenedioxythiophene (EDOT) and 100 mM $LiClO_4$, the above Co_3O_4 nanowire arrays as the working electrode, Ag/AgCl as the reference electrode and a Pt foil as the counter-electrode. The Co_3O_4/PEDOT core/shell nanowire arrays were prepared via electro-deposition for 500 s.

Characterization of Core-Branch Nanowire Arrays. The samples were characterized by X-ray diffraction (XRD, RIGAKU D/Max-2550 with Cu Kα radiation), field emission scanning electron microscopy (FESEM, FEI SIRION), high-resolution transmission electron microscopy (HRTEM, JEOL JEM-2010F) and X-ray photoelectron spectroscopy (XPS, PHI 5700). The surface area of the film that scratched from the substrate was determined by BET measurements using a NOVA-1000e surface area analyzer.

Electrochromic Measurements. The transmission spectra of coaxial TiO_2/PANI core/shell nanorod arrays in different redox states were measured over the range from 200 to 900 nm with a SHIMADZU UV-240 spectrophotometer. Each spectrum was recorded ex-situ after the samples taken out of the three-compartment system. The cyclic voltammetry (CV), chronoamperometry (CA) and electrochemical stability measurements of coaxial TiO_2/PANI core/shell nanorod arrays were carried out in a three-compartment system containing 0.1 M HCl as the electrolyte, Ag/AgCl as the reference electrode and a Pt foil as the counter-electrode on a Electrochemical Workstation (CHI760B, Chenhua, Shanghai). The CV measurements were carried out in the potential range of –0.2 to 1.0 V with a scanning rate of 50 mV s^{-1} at room temperature.

Li Ion Battery Measurements. CR2025 coin-type cells were directly fabricated from the coaxial Co_3O_4/PANI core/shell nanowire arrays on nickel foam as the working electrode (Co_3O_4 mass≈ 1.5 mg cm^{-2}, PANI mass≈0.12 mg cm^{-2}) without any ancillary materials. A metallic lithium foil served as the counter electrode, 1 M $LiPF_6$ in ethylene carbonate (EC)-dimethyl carbonate (DMC) (1: 1 in volume) was used as the electrolyte, and a polypropylene micro-porous film (Cellgard 2300) as the separator. The cells were assembled in an argon-filled glove box with high-purity argon gas (99.9995% purity). The galvanostatic charge-discharge tests were performed on LAND battery program-control test system (Wuhan, China) between 0 and 3 V at room temperature. Cyclic voltammetry (CV) and electrochemical

impedance spectroscopy (EIS) measurements tests were carried out on a CHI660C electrochemical workstation (Chenhua, Shanghai) and the CV test was conducted in the potential window of 0–3V (vs. Li/Li^+) at a scan rate of 0.1 mV s^{-1}.

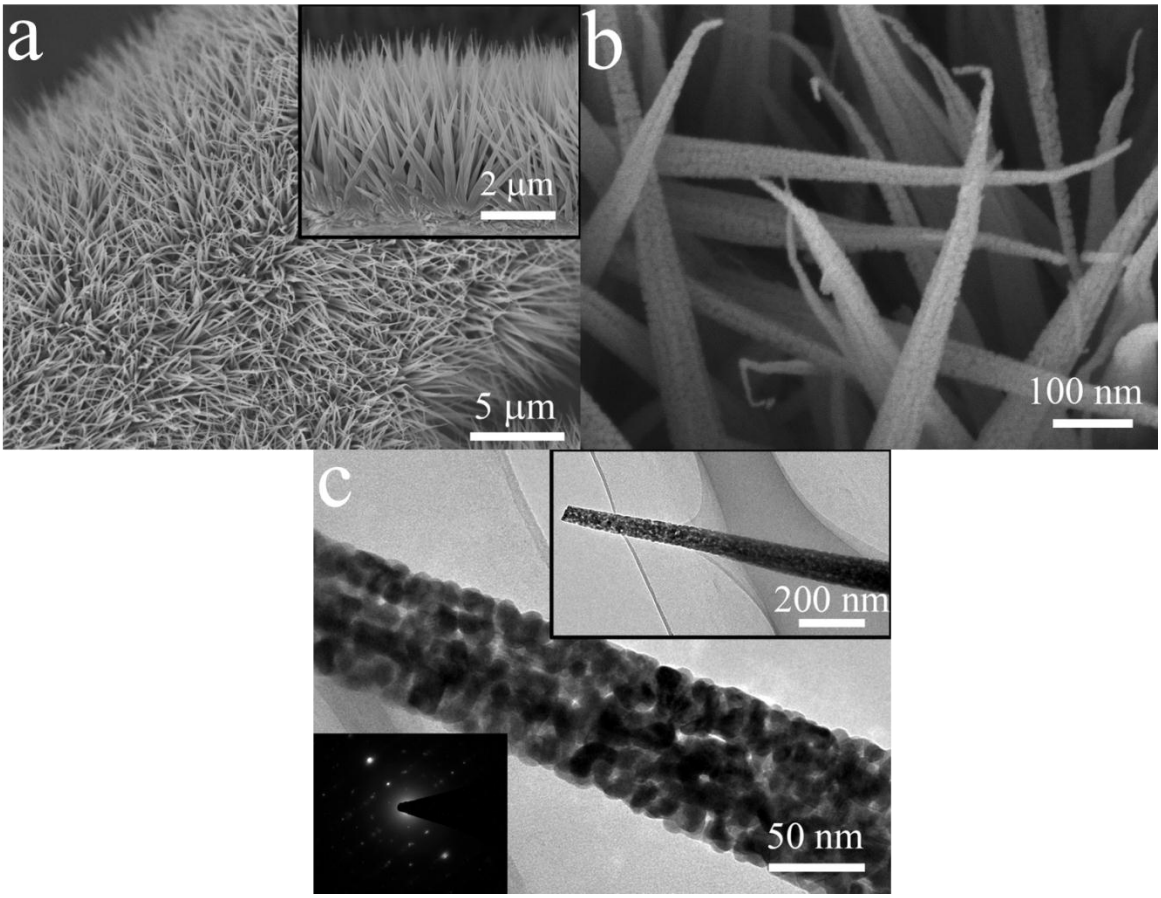

Figure S1 SEM-TEM images of Co_3O_4 nanowire arrays on carbon cloth (cross-sectional image, SAED pattern and low-magnification TEM image in inset)

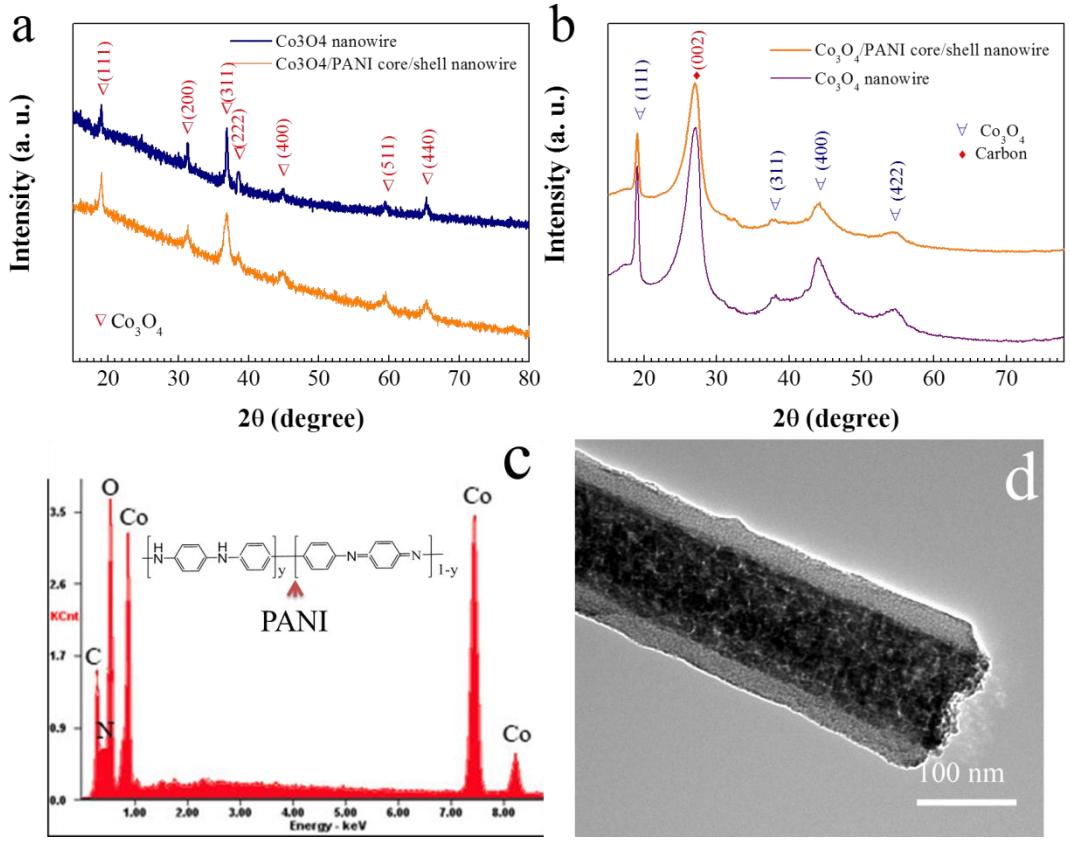

Figure S2 XRD patterns of Co_3O_4 and Co_3O_4/PANI core/shell nanowire arrays (a) powder sample scratched from the substrates and (b) on carbon cloth. (c) EDS spectrum of coaxial Co_3O_4/PANI core/shell nanowires scratched from the substrate (the molecular formula of PANI in inset). (d) TEM image of coaxial Co_3O_4/PANI core/shell nanowire.

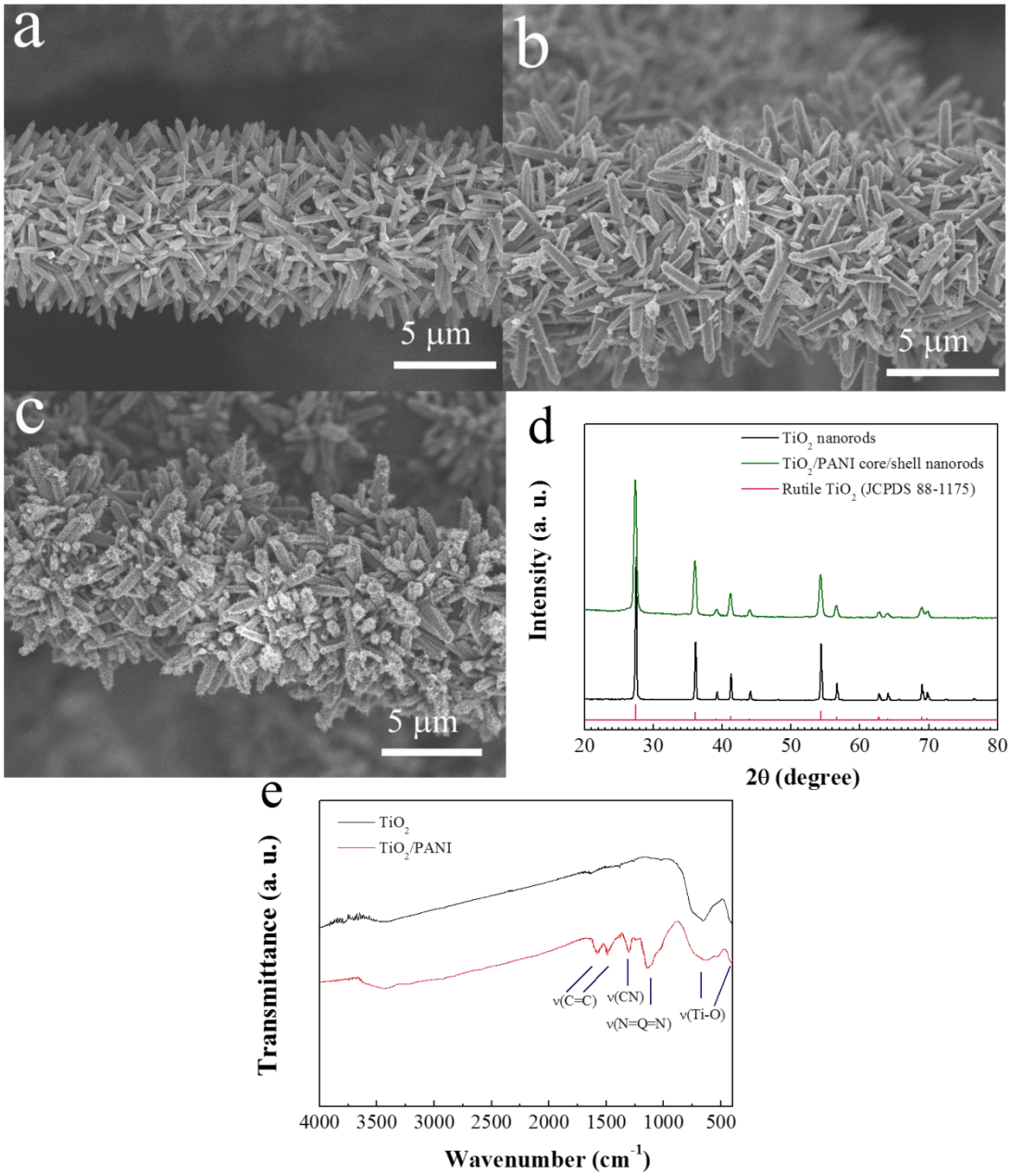

Figure S3 Low-magnification SEM images of (a) TiO_2 nanorod arrays, (b) coaxial TiO_2/PANI core/shell nanorod arrays and (c) branched TiO_2/PANI core/shell nanorod arrays on carbon cloth. (d) Powder XRD patterns of TiO_2 nanorods and TiO_2/PANI core/shell nanorod arrays scratched from the substrates. (e) FTIR spectra of TiO_2 nanorods and TiO_2/PANI core/shell nanorods scratched from the substrates. Both samples have peaks centered at 652 and 410 cm^{-1} characteristic of TiO_2. The other peaks belong to PANI.

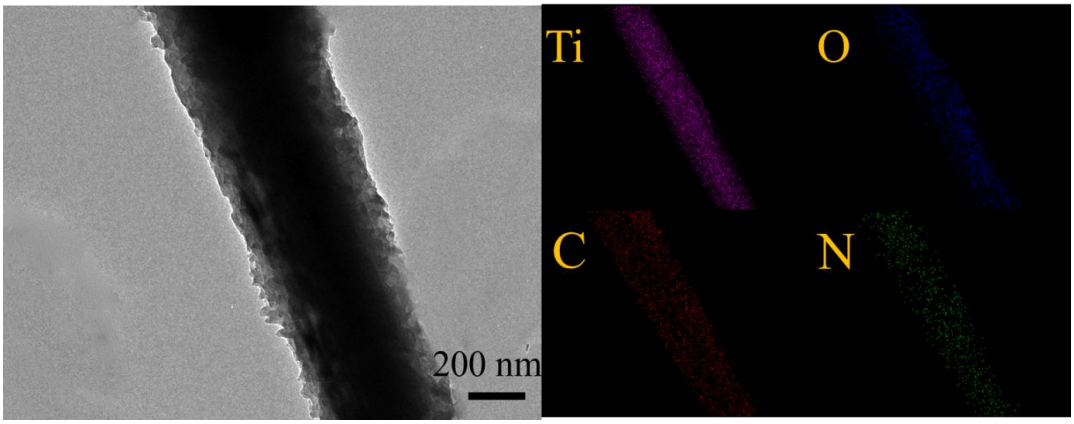

Figure S4 TEM image of coaxial TiO_2/PANI core/shell nanorod and corresponding EDS mapping.

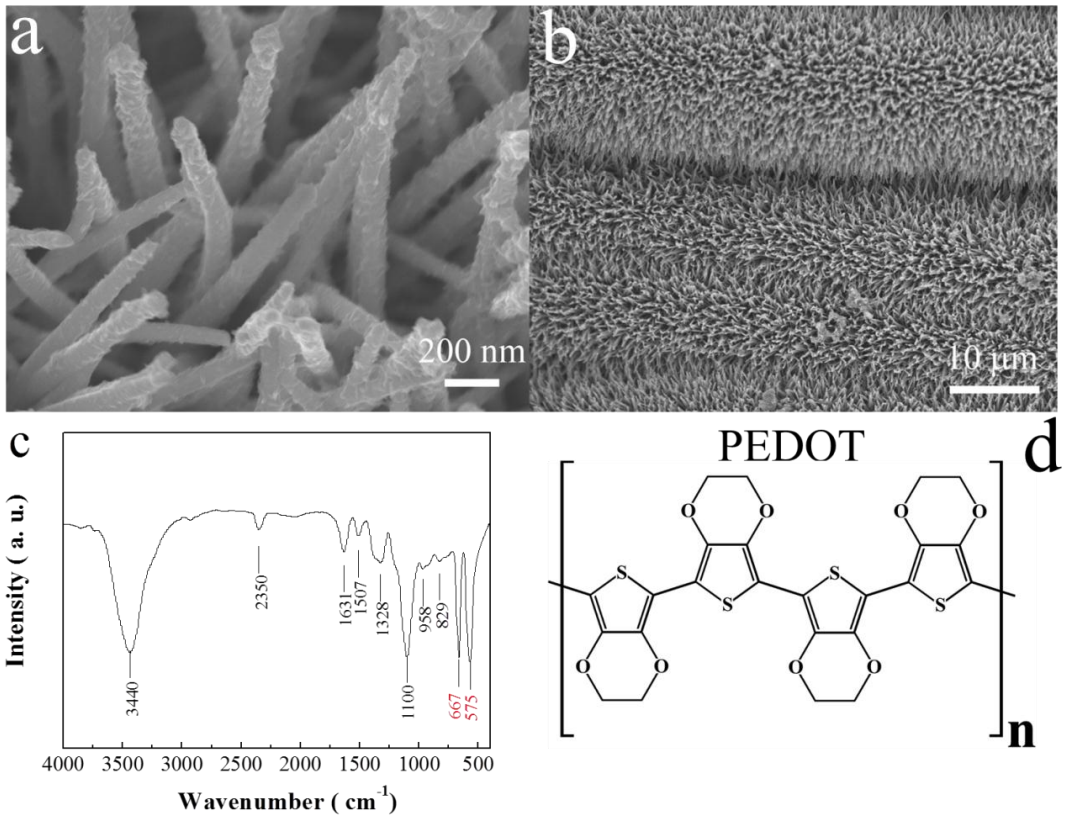

Figure S5. (a, b) SEM images of coaxial Co_3O_4/PEDOT core/shell nanowire arrays on carbon cloth and (c) corresponding FTIR spectrum. Except for two strong peaks at 667 and 575 cm^{-1} of Co3O4, other FTIR peaks belong to PEDOT. The peaks at 1507 cm^{-1} 1328 cm^{-1} correspond to the stretching vibration of C=C and C–C in the thiophene ring;[5] The band at 1100 cm^{-1} is due to the stretching vibrations of C–O–C; Three bands at 958 cm^{-1}, 829 cm^{-1} and 625 cm^{-1} is attributed to the vibrations of C–S in the thiophene ring. (d) Molecular formula of PEDOT.

Electrochemical impedance of metal oxide nanoarrays on carbon cloth

In our experiment, the working electrode must be conductive for the electrochemical deposition to take place. We have conducted resistance measurement of the Co_3O_4 nanowire, NiO nanoflake and TiO_2 nanorod on FTO glass by four points probe technique, respectively. The sheet resistance for the Co_3O_4 nanowire, NiO nanoflake and TiO_2 nanorod electrode is about 17, 38 and 163 Ω/square, respectively. (Note that the resistance is obtained from the overall electrode because these metal oxides nanoarray (nanowire, nanoflake and nanorod) grow vertically to the substrate and may not fully cover the FTO surface). It is found that the Co_3O_4 nanowire has the highest electrical conductivity, whereas the TiO_2 nanorod the lowest. In addition, we also conducted electrochemical impedance spectra (EIS) measurements of the Co_3O_4 nanowire, NiO nanoflake and TiO_2 nanorod arrays grown on carbon cloth in 1M KOH to reveal the electrical conductivity. The results are shown in Figure S6 as below.

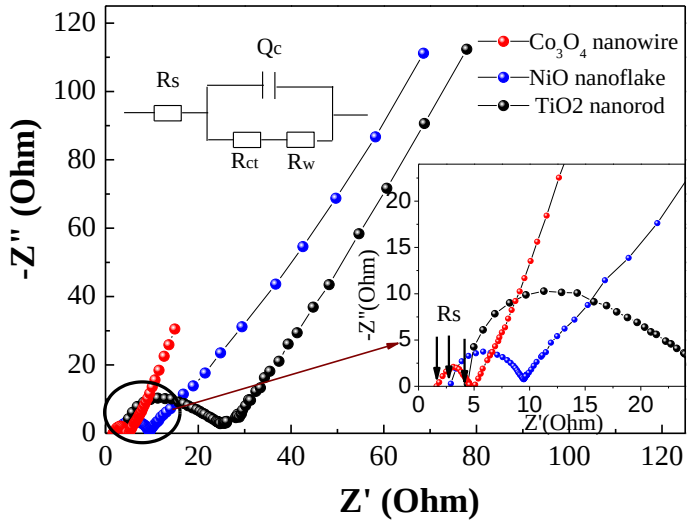

Figure S6. Nyquist plots of Co_3O_4 nanowire, NiO nanoflake and TiO_2 nanorod arrays grown on carbon cloth. Inset at top shows the equivalent circuit. R_s, Q_c, R_{ct} and Z_w denote the total ohmic resistance between the solution and electrodes, the capacitance of the double layer, the electrochemical reaction impedance and the Warburg impedance, respectively.

As seen in Figure S6, the impedances of all nanoarray electrodes consist of a depressed arc in high frequency regions and a straight line in low frequency regions. Generally, the semicircle is correlated to the electrochemical reaction impedance of the film electrode and

the straight line to the diffusion of the electroactive species. It is accepted that a bigger semicircle means a larger charge-transfer impedance R_{ct}. R_s is the resistance between the electrode and electrolyte, which is found from the starting point of the semicircle on the real axis. It can be seen from Figure S6 that, the overall electrical conductance can be sorted as Co_3O_4 nanowire > NiO nanoflake > TiO_2 nanorod.

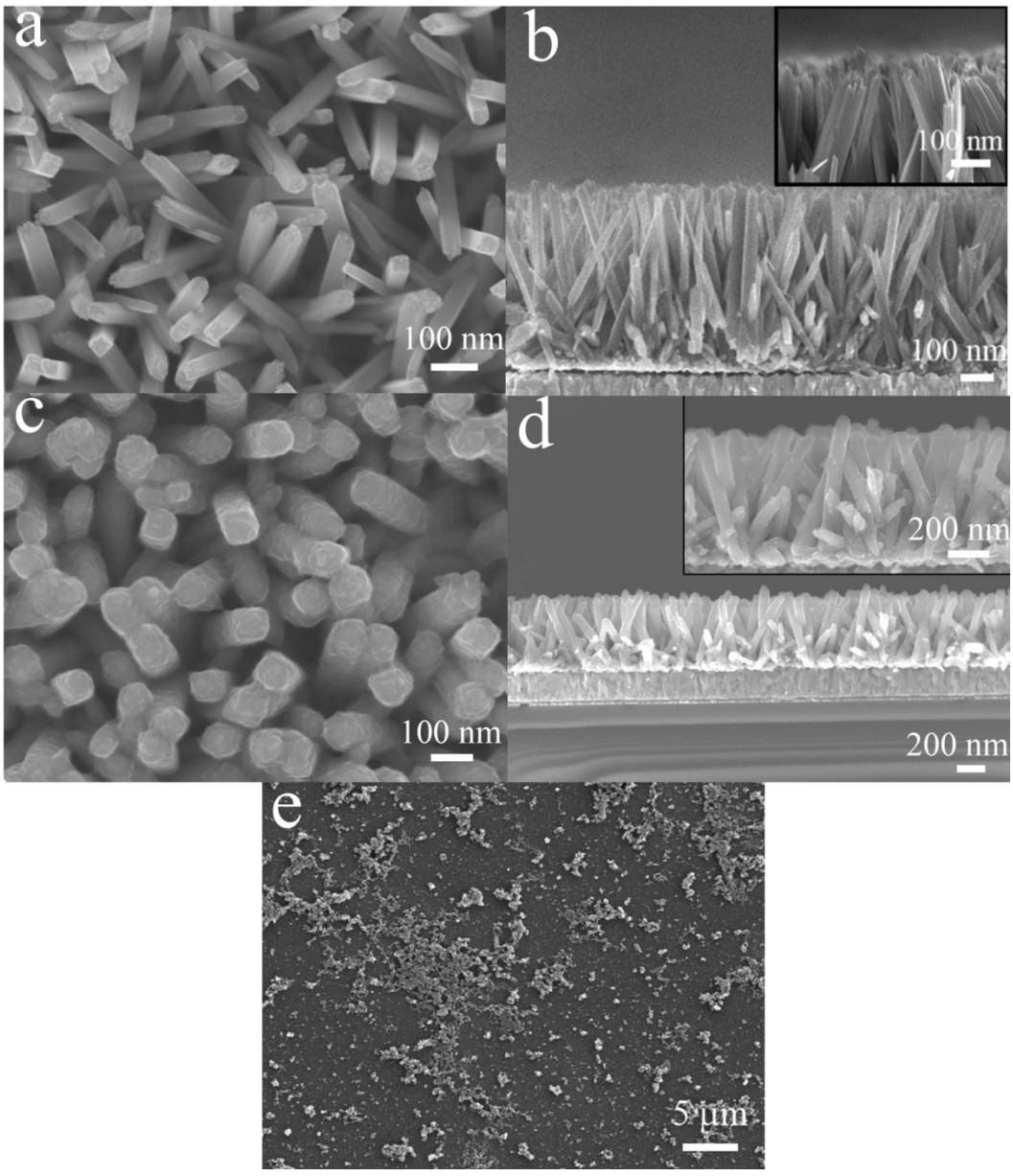

Figure S7. Top and side SEM images of (a, b) TiO_2 nanorod arrays on FTO and (c, d) coaxial TiO_2/PANI nanorod arrays on FTO. (e) Bare PANI on FTO.

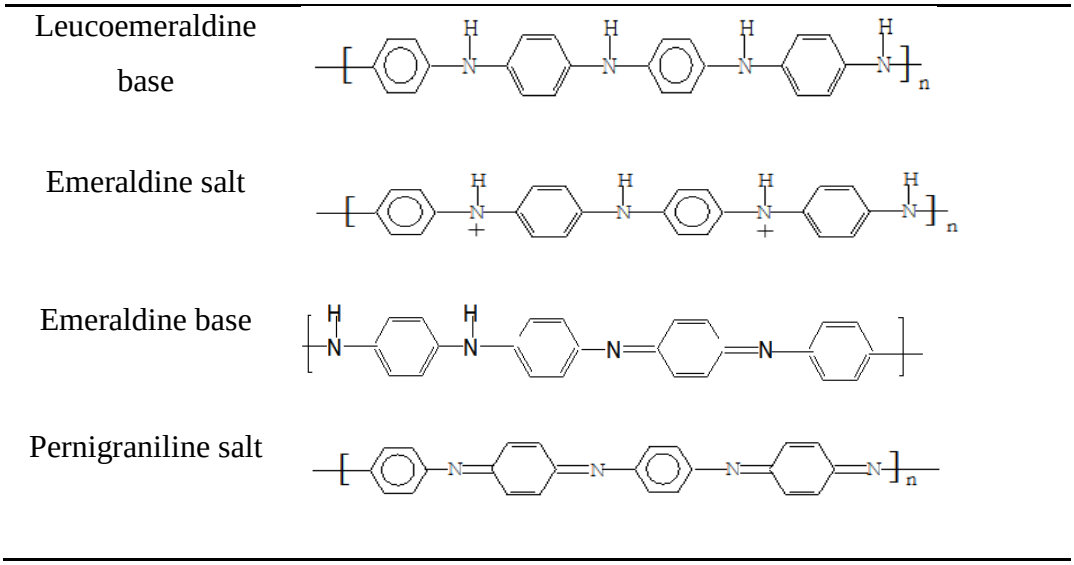

Figure S8. Main molecular structures of LB, ES, EB and PS.

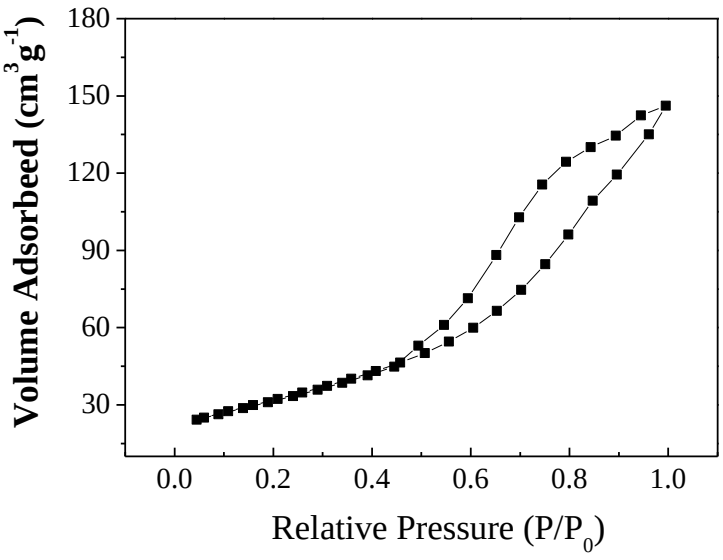

Figure S9. BET measurement of coaxial TiO_2/PANI core/shell nanorod arrays on FTO. The measured surface area is about 118 m^2 g^{-1}.

Li Ion Battery Measurements of Coaxial Co_3O_4/PANI Core/shell Nanowire Arrays.

As another demonstration of potential application, the coaxial Co_3O_4/PANI core/shell nanowire arrays are evaluated as the anode material for lithium ion batteries (LIB). Figure S10a shows the CV curves of the single Co_3O_4 nanowire and coaxial Co_3O_4/PANI core/shell nanowire arrays at a scanning rate of 0.5 mV s^{-1}. For the coaxial core/shell nanowire arrays, the reduction peaks at 0.70 V and 1.28 V correspond to the reduction of Co_3O_4 to metallic Co and the formation of a partially reversible solid electrolyte interphase (SEI) layer whose composition includes Li_2CO_3, ethyleneoxide-based oligomers, LiF, and lithium alkyl carbonate.[6-10] During the following anodic process, the oxidation peak at 1.70 V corresponds to the partial decomposition of the SEI, and the main oxidation peak located at 2.46 V corresponds to the decomposition of Li_2O leading to the reformation of Co_3O_4. For the single Co_3O_4 nanowire arrays, lower reduction peak potentials (0.58 V and 1.28 V) and higher oxidation peak potentials (1.81 V and 2.55 V) are noticed. Apparently, the core/shell nanowire arrays shorten the potential separation between the oxidation peak and the reduction peak. Additionally, the peak currents of the core/shell nanowire arrays are higher than those of the single Co_3O_4 nanowire arrays. *All these indicate that the coaxial Co_3O_4/PANI core/shell nanowire arrays have weaker polarization, better electrochemical activity and reaction reversibility than the single Co_3O_4 nanowire arrays*, supported by the electrochemical impedance spectroscopy (EIS) results (Figure S11).

The first discharge/charge profiles of both nanowire arrays at 1.5 A g^{-1} are shown in Figure S10b. The first discharge capacity of the coaxial Co_3O_4/PANI core/shell nanowire arrays is 1207 mAh g^{-1}, which is a little higher than that of the single Co_3O_4 nanowire arrays (1147 mAh g^{-1}). The first discharge capacities are higher than the theoretical value of Co_3O_4 (890 mAh g^{-1}), which is due to the formation of partially reversible SEI layer in the first discharge process. This phenomenon is also noticed in other transition metal oxides including Fe_2O_3, NiO, CoO and CuO.[6, 10-12] The first charge process of the coaxial Co_3O_4/PANI core/shell nanowire arrays exhibits a capacity of 953 mAh g^{-1} with an initial coulombic efficiency of 76.4 %. The capacity loss is mainly attributed to the incomplete decomposition of the SEI and Li_2O. In contrast, the single Co_3O_4 nanowire arrays present lower first charge capacity and initial coulombic efficiency (848 mAh g^{-1} and 73.9 %). Furthermore, notice that the core/shell nanowire arrays exhibits a higher discharge plateau and a lower charge plateau, indicating smaller potential hysteresis and lower internal resistance of the core/shell nanowire arrays, which is in agreement with the CV result.

The high-rate capabilities of both nanowire arrays are presented in Figure S10c. The coaxial Co_3O_4/PANI core/shell nanowire arrays deliver an average specific capacity of 918 mAh g^{-1} at 1.5 A g^{-1}, 834 mAh g^{-1} at 2 A g^{-1}, 726 mAh g^{-1} at 2.5 A g^{-1}, and 649 mAh g^{-1} at 3 A g^{-1}, respectively, higher than those of the single Co_3O_4 nanowire arrays (842 mAh g^{-1} at 1.5 A g^{-1}, 697 mAh g^{-1} at 2 A g^{-1}, 569 mAh g^{-1} at 2.5 A g^{-1}, and 453 mAh g^{-1} at 3 A g^{-1}). This clearly demonstrates the capability for high cycling rates. Moreover, the coaxial Co_3O_4/PANI core/shell nanowire arrays exhibit enhanced cycling life than the single Co_3O_4 nanowire arrays (Figure S10d), and present a specific capacity of 695 mAh g^{-1} at 1.5 A g^{-1}

after 50 cycles, higher than that of the single Co_3O_4 nanowire arrays (540 mAh g^{-1} at 1.5 A g^{-1}).

The sample structures after 50 cycles were checked by the SEM (Figure S10e and f). For the single Co_3O_4 nanowires, the whole structure disintegrates and the nanowires aggregate severely. This may block the electrolyte accessibility and cause activity deterioration on electrode materials. In contrast, this structural degradation is not observed in the coaxial Co_3O_4/PANI core/shell nanowire arrays and the intact morphology is well preserved after cycling process.

In our experiment, the as-prepared PANI shell is in the state of emeraldine salt (ES) with high conductivity (this can be easily controlled by preparation potential). The introduction of PANI into the core/shell nanowires constructs an integrated conductive network for the metal oxides (Co_3O_4) providing fast electron transfer, which is favorable for the improvement of electrochemical reactivity resulting in improved capacity and high-rate capability. Meanwhile, the molecular structure of PANI is easily to be infiltrated by the organic electrolyte and keep it in the molecular structure, and will not block the diffusion of Li ions. Furthermore, the PANI shell is just like a soft "armor" to protect the metal oxide core material. As a flexible organic material, the PANI shell may accommodate the strain of metal oxides during lithiation/delithiation cycles and alleviate the structure damage caused by volume expansion, leading to improved cycle life.

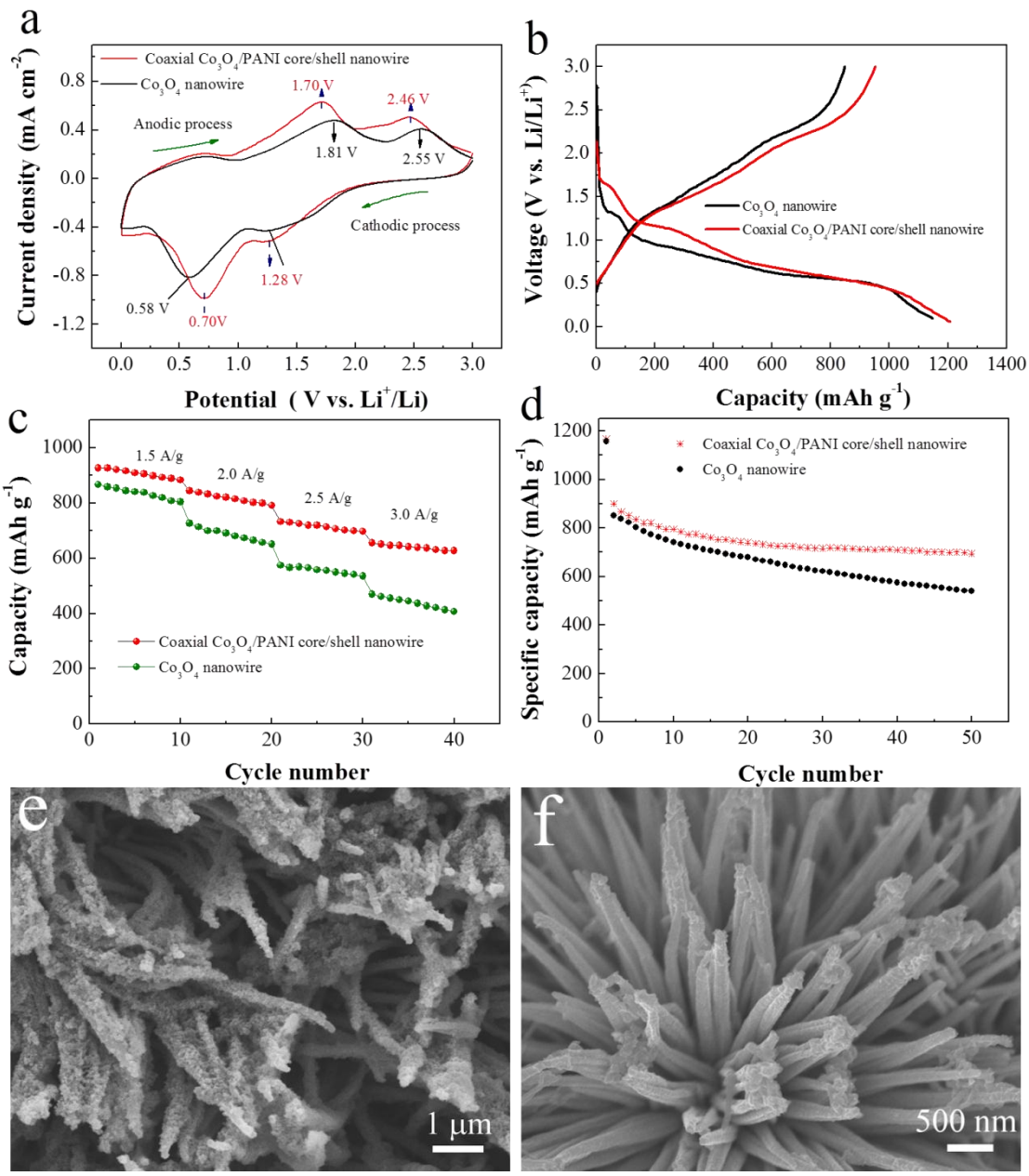

Figure S10. Comparison of electrochemical properties between Co_3O_4 nanowire and coaxial Co_3O_4/PANI core/shell nanowire arrays electrodes. (a) Cyclic voltammetry curves at a scanning rate of 0.5 mV s^{-1} at the second cycle. (b) Charge/discharge profiles at the current density of 1.5 A g^{-1} at the second cycle. (c) Rate performance in the current density range from 1.5 to 3 A g^{-1}. (d) Cycling performances at the current density of 1.5 A g^{-1}. SEM images of (e) Co_3O_4 nanowire and (f) coaxial Co_3O_4/PANI core/shell nanowire arrays electrodes after 50 cycles at 1.5 A g^{-1}.

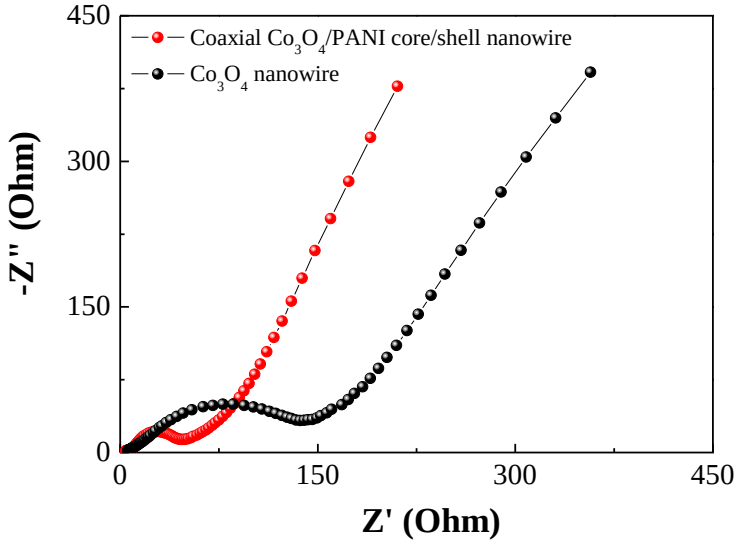

Figure S11. Nyquist plots of both nanowire arrays electrodes at 100 % depth of discharge at the 3nd cycle.

References for Supporting Information

(1) Xia, X. H.; Tu, J. P.; Zhang, Y. Q.; Wang, X. L.; Gu, C. D.; Zhao, X. B.; Fan, H. J. *ACS Nano* **2012,** *6*, 5531-5538.

(2) Liu, B.; Aydil, E. S. *J. Am. Chem. Soc.* **2009,** *131*, 3985-3990.

(3) Guan, C.; Li, X. L.; Wang, Z. L.; Cao, X. H.; Soci, C.; Zhang, H.; Fan, H. J. *Adv. Mater.* **2012,** *24*, 4186-4190.

(4) Yan, X. Y.; Tong, X. L.; Wang, J.; Gong, C. W.; Zhang, M. G.; Liang, L. P. *J. Alloys Compd.* **2013,** *556*, 56-61.

(5) Mumtaz, M.; Lecommandoux, S.; Cloutet, E.; Cramail, H. *Langmuir* **2008,** *24*, 11911-11920.

(6) Debart, A.; Dupont, L.; Poizot, P.; Leriche, J. B.; Tarascon, J. M. *J. Electrochem. Soc.* **2001,** *148*, A1266-A1274.

(7) Gachot, G.; Grugeon, S.; Armand, M.; Pilard, S.; Guenot, P.; Tarascon, J.-M.; Laruelle, S. *J. Power Sources* **2008,** *178*, 409-421.

(8) Grugeon, S.; Laruelle, S.; Herrera-Urbina, R.; Dupont, L.; Poizot, P.; Tarascon, J.-M. *J. Electrochem. Soc.* **2001,** *148*, A285-A292.

(9) Larcher, D.; Bonnin, D.; Cortes, R.; Rivals, I.; Personnaz, L.; Tarascon, J. M. *J. Electrochem. Soc.* **2003,** *150*, A1643-A1650.

(10) Taberna, L.; Mitra, S.; Poizot, P.; Simon, P.; Tarascon, J. M. *Nat. Mater.* **2006,** *5*, 567-573.

(11) Poizot, P.; Laruelle, S.; Grugeon, S.; Dupont, L.; Tarascon, J. M. *Nature* **2000,** *407*, 496-499.

(12) Débart, A.; Dupont, L.; Poizot, P.; Leriche, J.-B.; Tarascon , J. M. *J. Electrochem. Soc.* **2001,** *148*, A1266-A1274.